Hindawi Publishing Corporation
International Journal of Photoenergy
Volume 2014, Article ID 249317, 10 pages
http://dx.doi.org/10.1155/2014/249317

Research Article

Development of Thin Film Amorphous Silicon Tandem Junction Based Photocathodes Providing High Open-Circuit Voltages for Hydrogen Production

F. Urbain,[1] K. Wilken,[1] V. Smirnov,[1] O. Astakhov,[1] A. Lambertz,[1] J.-P. Becker,[1] U. Rau,[1] J. Ziegler,[2] B. Kaiser,[2] W. Jaegermann,[2] and F. Finger[1]

[1] *IEK-5 Photovoltaik, Forschungszentrum Jülich, 52425 Jülich, Germany*
[2] *Institute of Materials Science, TU Darmstadt, 64287 Darmstadt, Germany*

Correspondence should be addressed to F. Urbain; f.urbain@fz-juelich.de

Received 13 March 2014; Revised 24 June 2014; Accepted 30 June 2014; Published 16 July 2014

Academic Editor: Wenjun Luo

Hydrogenated amorphous silicon thin film tandem solar cells (a-Si:H/a-Si:H) have been developed with focus on high open-circuit voltages for the direct application as photocathodes in photoelectrochemical water splitting devices. By temperature variation during deposition of the intrinsic a-Si:H absorber layers the band gap energy of a-Si:H absorber layers, correlating with the hydrogen content of the material, can be adjusted and combined in a way that a-Si:H/a-Si:H tandem solar cells provide open-circuit voltages up to 1.87 V. The applicability of the tandem solar cells as photocathodes was investigated in a photoelectrochemical cell (PEC) measurement set-up. With platinum as a catalyst, the a-Si:H/a-Si:H based photocathodes exhibit a high photocurrent onset potential of 1.76 V versus the reversible hydrogen electrode (RHE) and a photocurrent of 5.3 mA/cm^2 at 0 V versus RHE (under halogen lamp illumination). Our results provide evidence that a direct application of thin film silicon based photocathodes fulfills the main thermodynamic requirements to generate hydrogen. Furthermore, the presented approach may provide an efficient and low-cost route to solar hydrogen production.

1. Introduction

Solar based hydrogen production via photoelectrochemical water splitting provides an alluring route to convert solar energy into a storable and clean chemical fuel and, therefore, increasingly plays a decisive role in sustainable energy concepts [1, 2]. Among the current variety of photoelectrode absorber materials for integrated water splitting devices, including III—V semiconductors [3–6], metal oxides [7–9], or crystalline silicon [10–12], amorphous silicon thin films emerge as a novel promising candidate [9, 13–16]. Overall, thin film silicon technology stands out as an attractive choice for water splitting applications, because it combines low-cost production, earth abundance, and versatility [17].

Amorphous silicon tandem solar cells have been intensively developed in the past, with major focus on high conversion efficiencies [18]. In our approach here, however, the focus is on the development of high V_{OC} devices, suitable for water splitting applications. Therefore, we will describe a development route to achieve high voltage devices and emphasize which particular parameter regimes are optimal in order to achieve high open-circuit voltages in a-Si:H/a-Si:H tandem junction solar cells. Additionally it will be shown that the parameters can be systematically adjusted to tune the V_{OC} values in the range between 1.60 V and 1.87 V, which is relevant if one considers various PEC systems with different overpotential losses, that is, when different voltage requirements are implied. The major part of the reported a-Si:H tandem solar cells for water splitting applications was merely designed to provide additional bias to a photoactive metal oxide electrode [9, 14, 16]. In contrast, this study reports on the direct application of the a-Si:H tandem solar cells as all-silicon photoelectrodes for driving the water splitting reactions.

Regarding solar assisted water electrolysis and the concomitant requirement of electrochemical potentials, that is,

photovoltages above 1.23 V (disregarding overpotentials) [19–21], photocathodes providing high photocurrent at high voltages are desirable. Concerning this, great importance is given to the versatility of the a-Si:H material. By changing deposition process parameters, the electronic and optical properties of the a-Si:H absorber material can be adjusted, such that a wide range of high open-circuit voltages is provided in a-Si:H based single junction solar cells, without significantly impairing current densities [22, 23]. In comparison, other photocathode material systems listed above often suffer from rather low photovoltages and therefore limit the solar to hydrogen efficiency. The open-circuit voltage of a properly designed solar cell mainly depends on the band gap of the absorber layer. Thus, attempts for the variation in band gap energy of intrinsic a-Si:H absorber layers were made in this study. In real photoelectrochemical assemblies, the potential losses inevitably exceed 200 mV, depending on the current densities and catalysts used [24, 25]. Thus, for self-contained solar water splitting devices photovoltages of at least 1.43 V are needed. In this manner, a-Si:H based solar cells are very beneficial, because the electronic properties of individual a-Si:H absorber layers can be combined by connecting two single junction cells (subcells) in series. In this configuration a-Si:H/a-Si:H tandem junction solar cells promote a further extended range of achievable high voltages [26, 27]. Thus, they may satisfy the specific thermodynamic requirements of different photoelectrochemical systems.

Based on (photo-)electrochemical experiments, the performance and stability of the developed a-Si:H/a-Si:H tandem junction based photocathodes were evaluated with respect to the hydrogen evolution reaction (HER). Moreover, to fully explore the performance of the photocathode, platinum was evaporated as a catalyst.

2. Experimental Details

2.1. Preparation of a-Si:H Layers and Solar Cells. All a-Si:H layers were deposited by a plasma enhanced chemical vapor deposition (PECVD) technique in a multichamber system. For the intrinsic a-Si:H absorber layers a mixture of silane (SiH_4) and hydrogen (H_2) gases was used. For the n- and p-type layers, trimethylborane (TMB), methane (CH_4), and phosphine (PH_3) gases were added to the silane-hydrogen mixture. An excitation frequency of 13.56 MHz was applied for all depositions. The a-Si:H material optimization was mainly performed as a function of the substrate temperature T_s and silane concentration SC, defined as the ratio between the SiH_4 flow and the total gas flow. Single junction and tandem junction solar cells were made in a p-i-n and in a p-i-n-p-i-n superstrate configuration, respectively, with a sputtered zinc oxide/silver (ZnO/Ag) reflecting back contact [28] defining the area (1 cm^2) of the individual cells. The thickness of the intrinsic a-Si:H layer in single junction solar cells was kept constant at 400 nm. In the standard tandem device, the bottom cell thickness was 400 nm and the top cell thickness was 110 nm. The p- and n-doped layers are the same for all fabricated solar cells and are deposited at a substrate temperature of 180°C. Since T_s is varied for the deposition of the intrinsic a-Si:H layer, a waiting time of 30 minutes between the layer deposition was implemented in order to maintain a required temperature of the substrate. All solar cells were deposited on 100 cm^2 fluorine-doped tin oxide (SnO_2:F) coated glass substrates with a native texture (Asahi U). Figure 1 schematically shows the tandem junction solar cell configuration used in the photovoltaic arrangement. For the investigation of the intrinsic a-Si:H layers alone, glass substrate (type Corning Eagle XG) and crystalline silicon wafers were used as substrates and all respective single a-Si:H layers had a thickness of approximately 500 nm. For the photoelectrochemical arrangement, 50 nm of platinum was deposited on the ZnO/Ag back contact by electron beam evaporation.

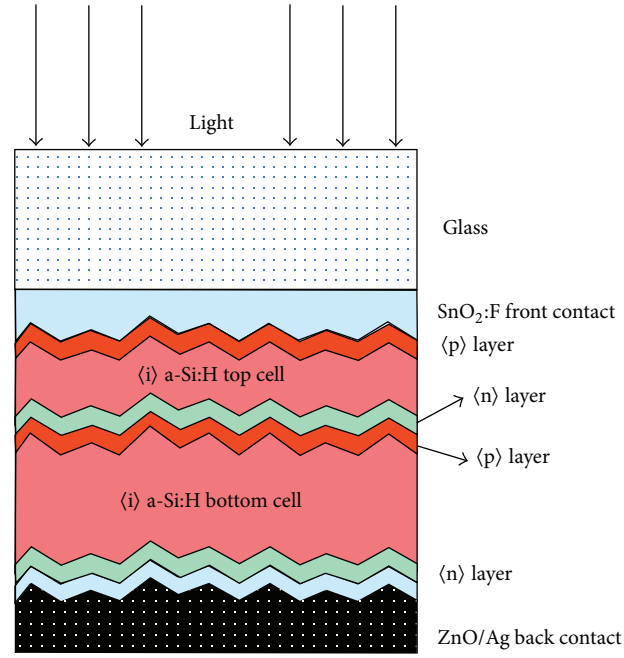

Figure 1: Schematic drawing of the layer stack used for the deposition of a-Si:H/a-Si:H tandem solar cells.

2.2. Characterization of Materials and Solar Cells. Infrared (IR) absorption measurements were carried out, using a Fourier transform spectrometer (type Nicolet 5700), to evaluate the hydrogen content c_H in the intrinsic a-Si:H layer. IR transmission was measured between 400 and 2400 cm^{-1}. This spectrum was normalized to the spectrum of the crystalline silicon wafer substrate.

Photothermal deflection spectroscopy (PDS) was performed to measure the absorption spectra of the intrinsic a-Si:H layers, which were deposited on glass substrates. From these spectra the gap energy E_{04} with a PDS absorption coefficient of 10^4 cm^{-1} was extracted, which serves as a measure for the optical band gap of the intrinsic a-Si:H layer.

The constant photocurrent method (CPM) was used to evaluate the absorption within the band gap (e.g., subgap absorption), which can be linked to the defect density of the a-Si:H material. The corresponding defect absorption densities

of the a-Si:H intrinsic layers were determined by using the absorption coefficient $\alpha_{1.2}$ at an energy of 1.2 eV [29].

Solar cells were characterized by current-voltage (J-V) measurements under AM 1.5 illumination using a double source (Class A) sun simulator and by quantum efficiency (QE) measurements.

2.3. Photoelectrochemical Measurements. The photoelectrochemical performance of the electrodes was evaluated at room temperature in an aqueous 0.1 M sulfuric acid (H_2SO_4) electrolyte solution (pH 1) using a three-electrode configuration [30]. The potential of the working electrode was controlled by a potentiostat (μAutolab Type III). For illumination, a 150 W xenon-halogen lamp was used, which was calibrated (by adjusting the current) with a crystalline silicon diode to provide a light intensity of 100 mW cm^{-2}. The solar cells were illuminated through the glass substrate. The set-up of the electrochemical cell (type Zahner PECC-2) consists of a Teflon cell body and three electrodes: a working electrode (optimized a-Si:H/a-Si:H tandem junction solar cell, 8 mm diameter), a coiled platinum wire as a counter electrode, and a Ag/AgCl reference electrode being in contact with 3 M sodium chloride (NaCl) [0.268 V versus normal hydrogen electrode (NHE)]. For simplicity, the entire set-up will be denoted as photoelectrochemical cell (PEC) arrangement hereafter. Cyclic voltammetry measurements were performed with a scan rate of 30 mV s^{-1}. Electrical contact to the SnO_2 coated substrate, that is, the front contact of the solar cell, was made by a silver paste.

3. Results and Discussion

3.1. Material Properties of Intrinsic a-Si:H Absorber Layer. Since the band gap of amorphous a-Si:H correlates with the hydrogen content of the material [22], FTIR measurements were conducted to estimate the amount of hydrogen in the samples. Figure 2 shows the hydrogen content as a function of the substrate temperature for a-Si:H layers with different silane concentrations. The general trend indicates that a decrease in T_s results in an increase of c_H. This behavior can be attributed to the increased desorption of hydrogen at higher substrate temperatures. As deposition temperature increases, the desorption of hydrogen atoms is energetically favored and thus less hydrogen is incorporated into the layer [31]. No clear dependency of c_H on the silane concentration in the chosen range was visible in FTIR data. The hydrogen content in all samples investigated is between 10.6% and 16.8%.

For the determination of the band gap energy of the a-Si:H material, absorption spectra for different T_s and SC are measured and subsequently evaluated, with respect to E_{04} as an estimation of the band gap. The evaluated E_{04} values for all samples are shown in Figure 3. In the considered temperature range the band gap energy E_{04} decreases by approximately 80 meV with increasing T_s for a given SC. Additionally, a slight dependency of the E_{04} on SC can be extracted. For constant T_s, an average difference of approximately 30 meV between SC of 4% and 10% was observed. Considering all

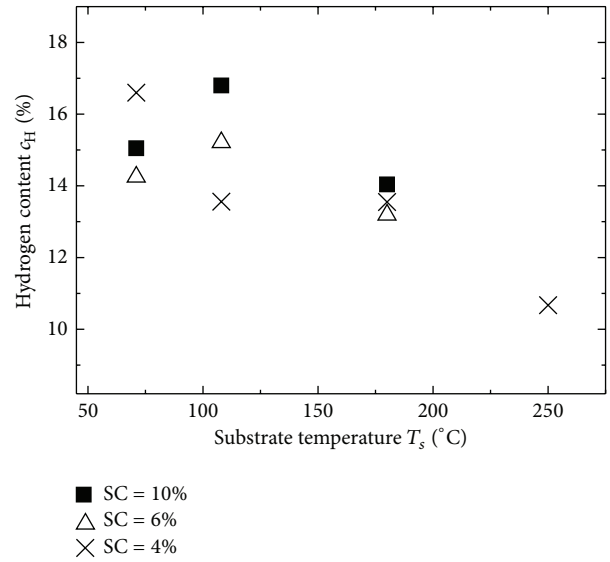

Figure 2: Hydrogen content as a function of the substrate temperature during deposition of the a-Si:H layers, with different silane concentrations.

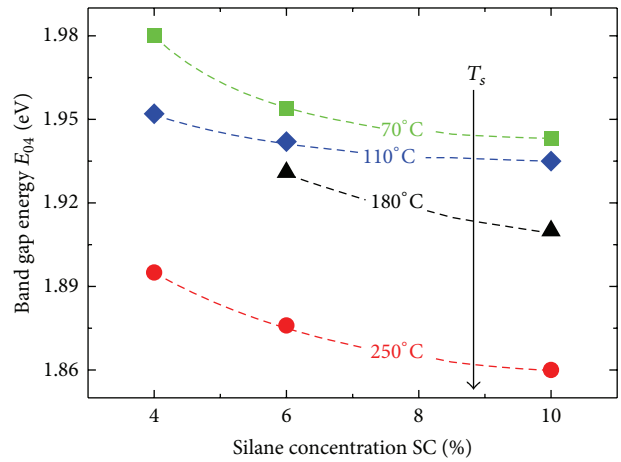

Figure 3: E_{04} band gap as a function of silane concentrations for a-Si:H layers deposited at different substrate temperatures T_s. The dotted lines are to guide the eye.

a-Si:H absorber layers, the optical band gap could be varied by 120 meV from 1.86 eV to 1.98 eV.

Figure 4 presents the evaluated E_{04} values as a function of c_H for different silane concentrations. The data of this study is in line with the commonly observed trend for an increase of the band gap energy with increasing fraction of bound hydrogen in the a-Si:H material [32–34]. A possible explanation suggested that the hydrogen could be involved in breaking of weak Si–Si bonds responsible for the states in the top of the valence band. As a consequence, by increasing c_H, stronger Si–H bonds emerge, leading to states deep in the valence band and resulting in the valence band edge being shifted down. The conduction band remains unaffected and thus, the band gap energy increases [22, 32]. Other microscopic models involve a discussion of the effects of nanosized

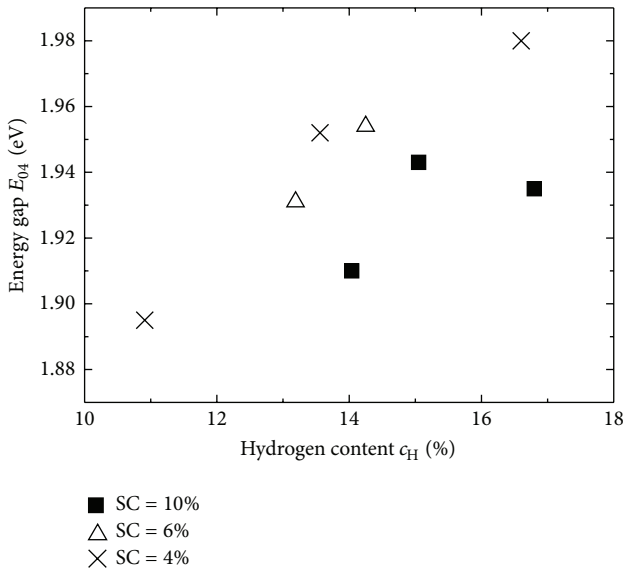

Figure 4: Band gap energy E_{04} as a function of the hydrogen content of deposited a-Si:H layers with different silane concentrations.

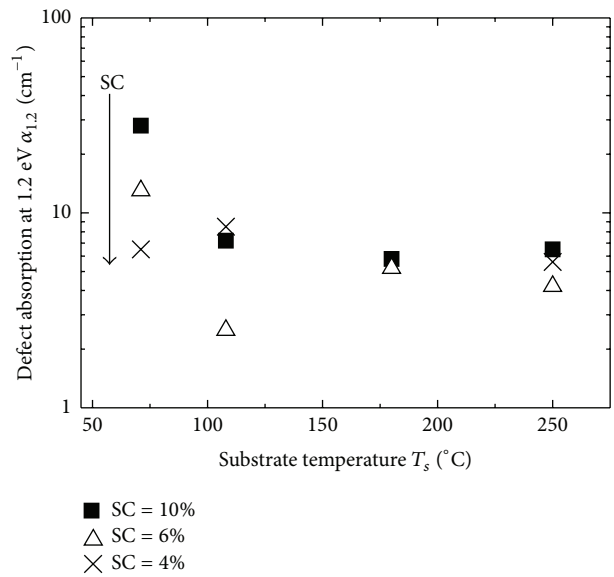

Figure 5: Absorption coefficient at 1.2 eV as a function of substrate temperature for different silane concentrations of the intrinsic a-Si:H layer.

void configurations on the hydrogen incorporation in a-Si:H material [35, 36].

The defect density is an important parameter for absorber materials, because electronic defects can act as recombination centers and lead to a deterioration of the device performance [37, 38]. In general, it is well accepted that a reduction in the deposition temperature (below 250°C) results in the increase in the defect density of a-Si:H material [31]. Here, by adjusting SC together with T_s, we can maintain a material with a reasonable electronic quality (low defect density) even at a very low deposition temperature of around 70°C. Figure 5 shows the absorption at an energy of 1.2 eV as a function of T_s for different SC of the a-Si:H layers. It is apparent that for substrate temperatures between 110°C and 250°C the absorption in the subgap region is similar for different silane concentrations investigated here and $\alpha_{1.2}$ ranges between 4.2 cm^{-1} and 8.5 cm^{-1}. At a temperature of 70°C, a distinct trend of decreasing $\alpha_{1.2}$ with decreasing silane concentration was observed. The defect absorption in this region rapidly increases up to 28 cm^{-1} for SC of 10%. By reducing SC of the a-Si:H layers deposited at 70°C, $\alpha_{1.2}$ continuously decreases to 6.5 cm^{-1} for SC of 4%. This value is similar to $\alpha_{1.2}$ values of the layers deposited at higher temperatures. Hence, this result emphasizes that the electronic quality of the a-Si:H material deposited at low substrate temperatures (around 70°C) can be improved, in terms of defect absorption density, by using lower silane concentrations during the deposition. We note that even at low SC of 4%, the materials are still fully amorphous as evident from the Raman scattering experiments.

3.2. Solar Cells

3.2.1. Single Junction Solar Cells. The investigated intrinsic a-Si:H absorber layers with different band gaps were subsequently applied in single junction solar cells in a p-i-n configuration. The solar cells were prepared with intrinsic a-Si:H layers at silane concentrations of 4% and 10%, in order to consider the entire range of E_{04} absorber layer band gaps (from 1.86 eV to 1.98 eV) for the relevant temperatures, shown in Figure 3.

The performance of the a-Si:H solar cells as a function of T_s is shown in Figure 6. Reducing T_s from 250°C down to 110°C, the open-circuit voltage V_{OC} increases with decreasing T_s and can be varied from 802 mV up to a value of 946 mV, achieved in the case of an absorber layer with SC of 4% and T_s of 130°C (Figure 6(b)). In this temperature range (250°C–110°C), the fill factor FF is only slightly affected and varies between 68.5% and 73.8% for SC of 10% and between 70.2% and 74.2% for SC of 4% (Figure 6(c)). The best efficiency η of 10.3% is obtained with an intrinsic a-Si:H layer with SC of 10%, deposited at 180°C (Figure 6(a)).

For even lower T_s of 70°C all performance parameters tend to deteriorate considerably, as compared with the solar cells deposited at T_s of 110°C or above. In the 70°C temperature region increased defect absorption density $\alpha_{1.2}$ (Figure 5.) and higher optical band gap E_{04} (Figure 3) significantly impair the electronic material quality. Nevertheless, as already apparent in the previous section, through the use of lower SC during low-temperature deposition, a significant improvement of the optoelectronic properties of a-Si:H material can be achieved. When SC is reduced down to 4%, a significant improvement in V_{OC} and FF is observed in the case of solar cells deposited at temperatures below 180°C. At T_s of 70°C and SC of 4%, all parameters are enhanced, compared to the 70°C cell with SC of 10%, and η yields 7.7% (Figure 6(a)). This underlines that a combination of low deposition temperature together with reduced SC of the absorber layer is necessary to obtain high voltage solar cells with appropriate efficiency level.

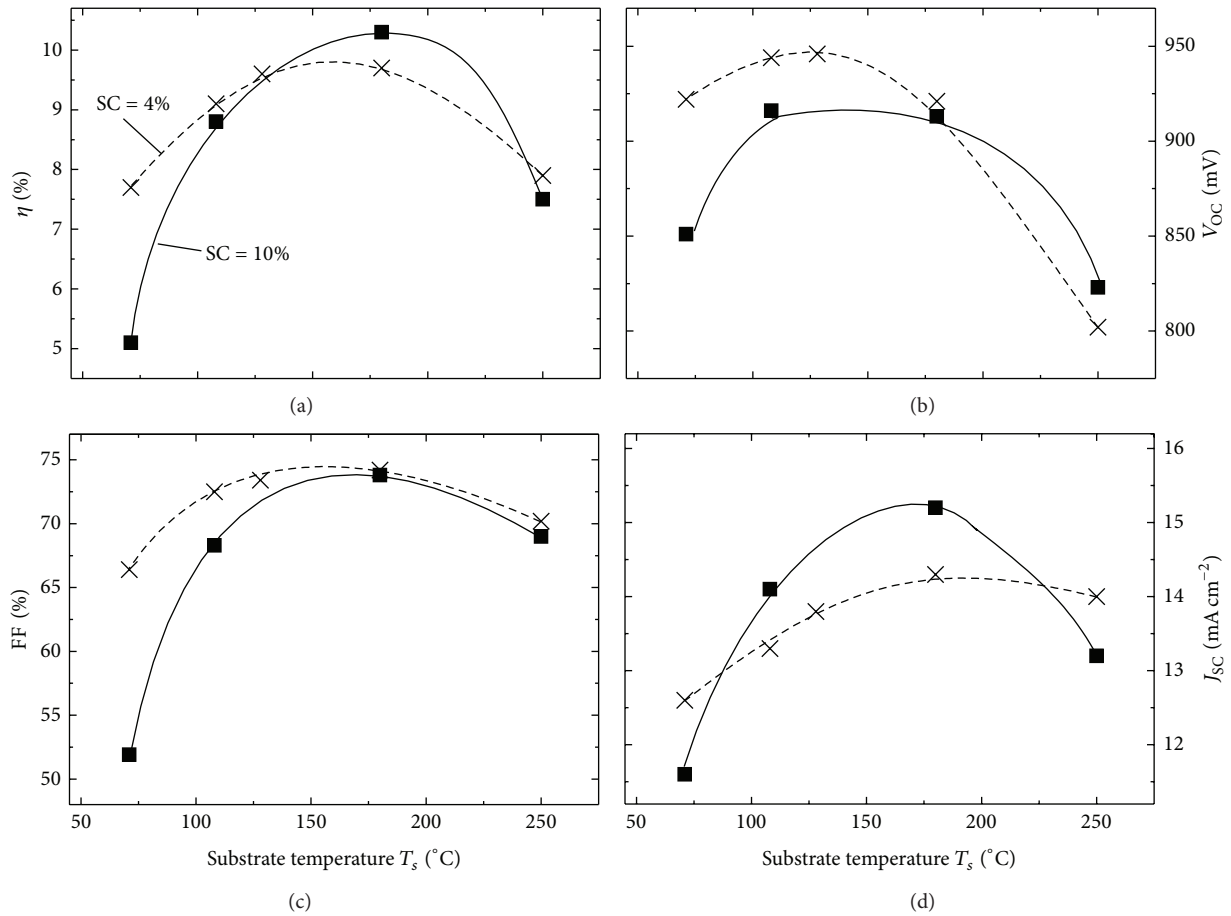

Figure 6: Photovoltaic parameters of single junction solar cells (efficiency (a), open-circuit voltage (b), fill factor (c), and short circuit current density (d)) as a function of the substrate temperature of the intrinsic a-Si:H layer, with 10% and 4% silane concentration, respectively. The lines are to guide the eye.

Figure 6(d) presents the J_{SC} data of the solar cell series as a function of T_s. From 70°C to 180°C, J_{SC} increases with increasing T_s and, except for T_s of 70°C, solar cells with SC of 10% promote higher J_{SC} compared to cells with SC of 4%. This can be explained by the wider E_{04} gap of a-Si:H layers with SC of 4%, in comparison to layers with SC of 10% (Figure 3). For T_s of 250°C however, J_{SC} decreases for both SC.

The quantum efficiencies for the solar cell series (the same as in Figure 6) deposited at SC of 4% and 10% at different T_s are shown in Figures 7(a) and 7(b), respectively. In the longer wavelength region the expected increase in QE with increasing T_s (i.e., decreasing E_{04}) is apparent for both SC. The QE in the shorter wavelength region reflects the trend of J_{SC} data shown in Figure 6(d). Thus, the decrease in total J_{SC} for T_s of 250°C (Figure 6(d)) is caused by the drop in current under short wavelength illumination and can be localized to the region of the solar cell where light of short wavelengths is mainly absorbed, that is, the region of the p-doped/intrinsic a-Si:H layer interface. At T_s of 250°C for the deposition of the intrinsic absorber layer, boron diffusion from the p-doped layer (deposited at 180°C) into the intrinsic a-Si:H layer is assisted, leading to a deterioration of the p-/i-interface, which can result in a reduction of the short wavelength QE [39]. In addition, as can be deduced from Figure 7(a), the QE for T_s of 70°C deteriorates over the entire wavelength range at SC of 10% but can be improved considerably by using a lower SC of 4% during the deposition of the intrinsic a-Si:H layer (Figure 7(b)).

3.2.2. Tandem Junction Solar Cells. Several tandem junction combinations of two a-Si:H single junction solar cells have been realized. The top and bottom cell combinations along with the absorber layer parameters (SC and T_s) and photovoltaic device parameters are listed in Table 1. The bottom cell thickness was 400 nm and the top cell thickness was 110 nm, respectively, for all the tandem junction cells from Table 1.

The data in Table 1 confirms that a broad range of high open-circuit voltages can be achieved, ranging from 1601 mV to 1870 mV. In addition, the V_{OC} values of the tandem solar cells are in good agreement with the summed V_{OC} values of the respective individual subcells, proving a stable process control. To ensure efficient hydrogen production, the a-Si:H/a-Si:H photocathode should preferably provide high photocurrent and operate near its maximum power point (MPP) during photoelectrochemical water splitting. Thus, J_{SC} and V_{MPP} play an important role here. In this regard, the

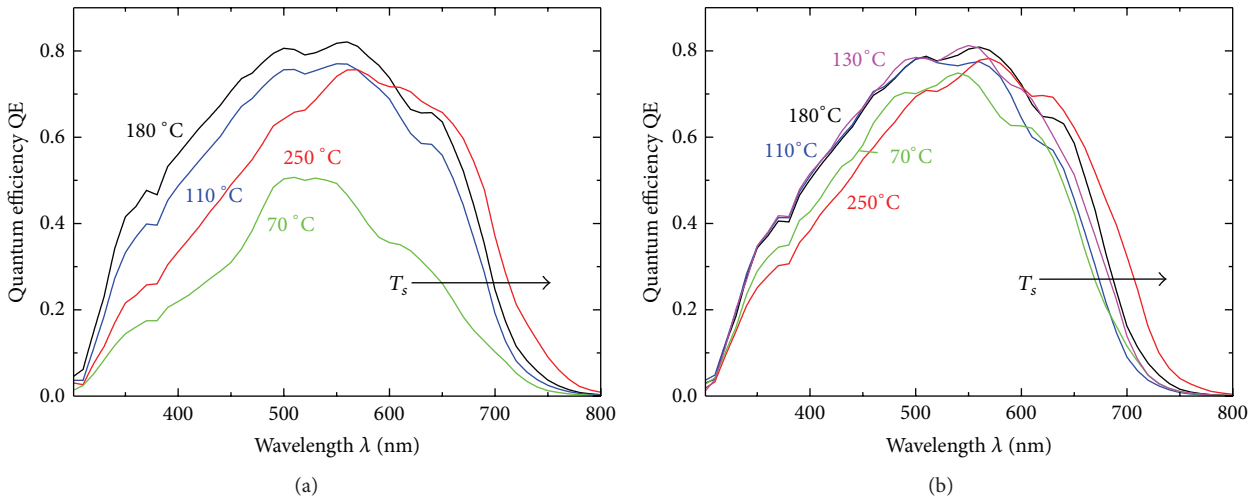

FIGURE 7: Quantum efficiency curves for single junction solar cells at silane concentration of (a) 10% and (b) 4% for different T_s of the absorber layer.

TABLE 1: Photovoltaic parameters of a-Si:H/a-Si:H tandem junction solar cells fabricated with varying SC and T_s of top and bottom cell.

Top cell		Bottom cell						
SC_{top} [%]	$T_{s,top}$ [°C]	SC_{bot} [%]	$T_{s,bot}$ [°C]	η [%]	V_{OC} [mV]	FF [%]	J_{SC} [mA/cm^2]	V_{MPP} [mV]
4	250	4	250	8.3	1602	71.8	7.2	1325
10	180	4	250	8.7	1700	68.5	7.4	1410
4	110	4	110	9.5	1870	77.5	6.6	1580
10	180	10	180	9.8	1796	78.8	7	1555
4	130	10	180	10.5	1816	73.5	7.9	1520
4	130	4	130	9.7	1855	78.2	6.7	1595

best two tandem cells listed in Table 1, with respect to J_{SC} and V_{MPP}, were chosen to be further optimized by means of current matching. The MPP voltage for all tandem cells is presented in the last column of Table 1. The highest V_{MPP} of 1595 mV is achieved by the tandem cell combining two subcells with SC of 4% and both $T_{s,top}$ and $T_{s,bot}$ of 130°C. The tandem cell consisting of a 4% SC top cell with $T_{s,top}$ of 130°C and a 10% SC bottom cell with $T_{s,bot}$ of 180°C exhibits the highest J_{SC} of 7.9 mA/cm^2 and an η of 10.5%.

In order to match the two subcells, with respect to the current, the thickness of the absorber layer of the top cell d_{top} has been optimized. The two chosen tandem cells were deposited with d_{top} of 70 nm and 90 nm, respectively, and compared with the tandem cell comprising the 110 nm thick top cell. Figure 8 presents the respective photovoltaic parameters as a function of the top cell thickness.

The matching series of the tandem cells with top and bottom absorber layers deposited at different T_s and SC (filled squares in Figure 8) shows that V_{OC} was only marginally affected by a reduced top cell thickness and increased by 15 mV for d_{top} of 110 nm to 70 nm (Figure 8(b)). The J_{SC} decreased with decreasing d_{top} from 7.9 mA/cm^2 for d_{top} of 110 nm to 6.7 mA/cm^2 for d_{top} of 70 nm (Figure 8(d)). As current matching should enhance the J_{SC} [40], one can conclude that the tandem cell was better matched at d_{top} of 110 nm and became top cell limited by further reducing d_{top}. The fill factor is expected to decrease when top and bottom cells are matched [39]. This is observed in Figure 8(c) where FF decreased by 4.9% with increasing d_{top}. The highest η of 10.5% was achieved when bottom and top cell are current matched (Figure 8(a)).

In the matching series of the second tandem cell, in which both top and bottom cell were deposited at T_s of 130°C and SC of 4% (open squares in Figure 8), the reduction of d_{top} leads to an increase in J_{SC} of 0.4 mA/cm^2 from d_{top} of 110 nm to 70 nm (Figure 8(d)). The FF decreased by 2.6% with decreasing d_{top} (Figure 8(c)). The highest V_{OC} of 1871 mV was achieved for the tandem cell with d_{top} of 90 nm (Figure 8(b)), which also exhibits the highest η of 9.9%.

The best two tandem cells, with respect to η, are summarized in Table 2.

3.3. Photoelectrochemical Measurements. The performance of the developed a-Si:H/a-Si:H tandem junction based photocathodes was examined and compared to the photovoltaic performance of the corresponding solar cells. For this purpose, four tandem cells covering up the V_{OC} range from 1600 mV to 1870 mV (from Tables 1 and 2) were chosen and the onset potential for cathodic current (E_{onset}), the potential at maximum power point (E_{MPP}), and the photocurrent density at 0 V versus RHE (J_{RHE}) were determined. Table 3

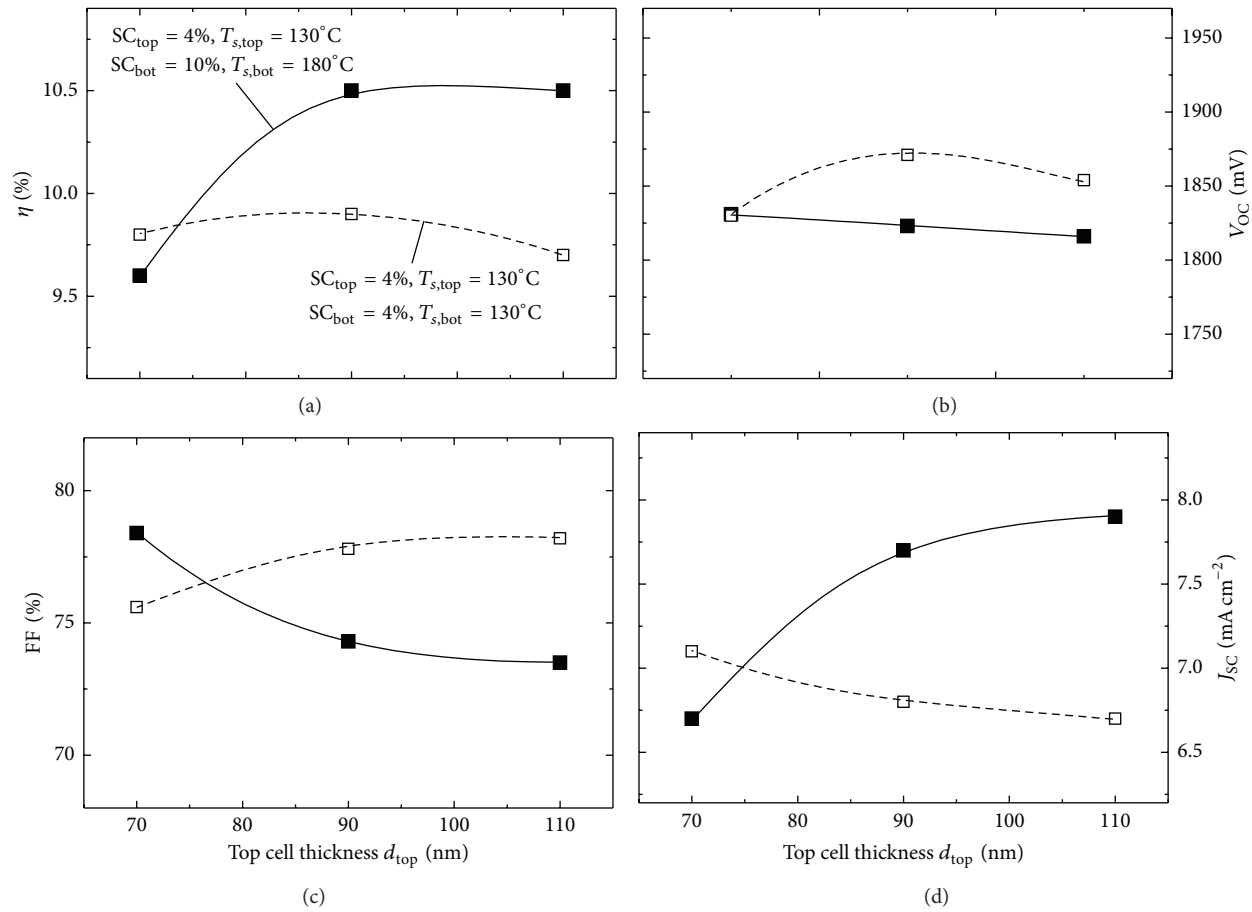

Figure 8: Photovoltaic parameters of the current matching series of two tandem junction solar cells deposited at different SC and T_s, as a function of their top cell thickness. The lines are to guide the eye.

Table 2: Photovoltaic parameters of a-Si:H/a-Si:H tandem junction solar cells resulting from the current matching series.

Top cell		Bottom cell						
SC$_{top}$ [%]	$T_{s,top}$ [°C]	SC$_{bot}$ [%]	$T_{s,bot}$ [°C]	η [%]	V_{OC} [mV]	FF [%]	J_{SC} [mA/cm^2]	V_{MPP} [mV]
4	130	10	180	10.5	1816	73.5	7.9	1520
4	130	4	130	9.9	1872	77.8	6.8	1600

provides the photovoltaic and PEC device parameters of the respective photocathodes. E_{MPP} and J_{RHE} (from Table 3.) are extracted from cyclic voltammetry (CV) measurements depicted in Figure 9. The measurements were conducted with the four a-Si:H/a-Si:H photocathodes without any further surface or back contact modification.

The disparity in J_{SC} and J_{RHE} values originates from the different illumination source used in photovoltaic and PEC arrangement, respectively. AM 1.5 illumination provides higher light intensities in the wavelength range between 300 nm and 800 nm, where a-Si:H possesses the highest light absorption, compared to the halogen lamp used in the PEC arrangement. Notwithstanding this, photovoltaic and photoelectrochemical performances show the same trends. The higher the V_{MPP} of a photocathode is, the higher its E_{MPP} is. A similar correlation was observed for the current densities J_{SC} andJ_{RHE}. This result provides evidence that the photoelectrochemical performance of the photocathode can be partly deduced from the photovoltaic performance of the solar cell, which is highly important for further development.

Photocathode D exhibits the highest photocurrent density of 6.3 mA/cm^2 at 0 V versus RHE. E_{MPP} of photocathode D is 1098 mV versus RHE and thus slightly lower than the highest E_{MPP} value of 1127 mV versus RHE and is promoted by photocathode C, which in contrast has a lower J_{RHE} of 5.3 mA/cm^2. The onset potential of cathodic current was taken as the value at a photocurrent density of −0.5 mA/cm^2. Hereby, E_{onset} data (from Table 3) reflects V_{OC} data obtained in photovoltaic arrangement and shifts anodically from photocathodes A and B (1196 mV versus RHE and 1338 mV versus RHE, resp.) to photocathodes D and C (1450 mV versus RHE and 1495 mV versus RHE, resp.). Efficient self-contained solar water splitting requires a photocathode with high photocurrent at a positive potential over 1.23 V versus

Table 3: Photovoltaic and PEC parameters of a-Si:H/a-Si:H tandem junction based photocathodes.

Photocathode	η [%]	V_{OC} [mV]	FF [%]	J_{SC} [mA/cm^2]	V_{MPP} [mV]	E_{onset} [mV versus RHE]	E_{MPP} [mV versus RHE]	J_{RHE} [mA/cm^2]
A	8.3	1602	71.8	7.2	1325	1196	832	5.9
B	8.7	1700	68.5	7.4	1410	1338	960	6.1
C	9.9	1872	77.8	6.8	1600	1495	1127	5.3
D	10.5	1816	73.5	7.9	1520	1450	1098	6.3

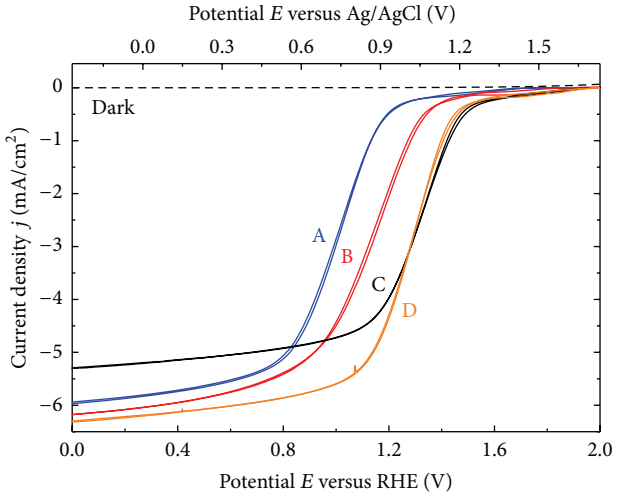

Figure 9: Cyclic voltammetry measurement of a-Si:H/a-Si:H photocathodes (listed in Table 3). Measurements were performed in 0.1 M H_2SO_4 solution (pH 1) under 100 mW/cm^2 illumination intensity at a scan rate of 30 mV s^{-1}. The dark current is shown as a black dashed curve.

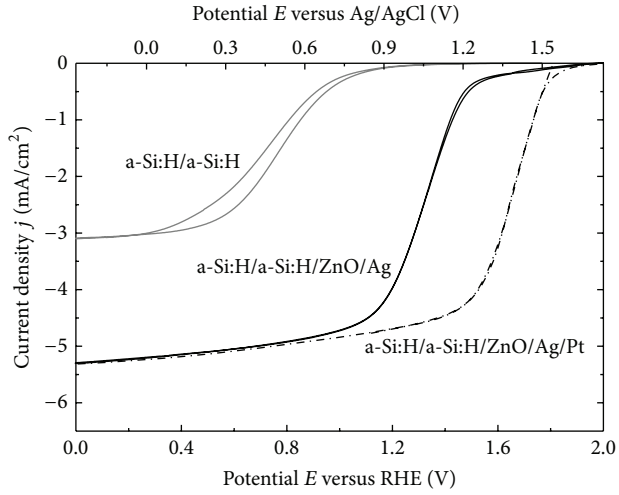

Figure 10: Cyclic voltammetry measurement of a-Si:H/a-Si:H photocathodes with no metallic back contact (solid grey curve), with ZnO/Ag back contact (solid black curve, photocathode C from Table 3) and with ZnO/Ag/Pt back contact (dashed curve), in 0.1 M H_2SO_4 solution (pH 1) under 100 mW/cm^2 illumination intensity at a scan rate of 30 mV s^{-1}.

RHE [13]. Thus, within this study photocathodes C and D are the most suitable candidates for PEC water splitting devices.

To describe the effect of different back contact catalysts, photocathode C was further investigated, as it exhibits the highest E_{onset}. Figure 10 shows the cyclic voltammograms measured for a-Si:H/a-Si:H photocathodes with no metallic back contact (solid grey curve, silicon in contact to the electrolyte), with ZnO/Ag back contact (solid black curve, photocathode C from Table 3) and with ZnO/Ag/Pt back contact (dashed curve). The low photocurrent (3.1 mA/cm^2 at 0 V versus RHE) of the back contact-free photocathode is caused by optical losses, due to the missing metallic back-reflector. Additionally, the injection of charge carriers into the electrolyte is kinetically limited for metal-free surfaces, resulting in high overpotentials for water reduction [24]. This is confirmed by the significant shift of E_{onset} in negative bias direction (950 mV versus RHE). Unlike the photocathodes with metallic back contacts, forward and reverse scan of the bare a-Si:H/a-Si:H photocathode are shifted, revealing a protective or passivation effect of the metallic back contact [12]. No effect on J_{RHE} is observed when a thin 50 nm layer of platinum is deposited on the ZnO/Ag back contact. Both photocathodes with metallic back contact provide 5.3 mA/cm^2 at 0 V versus RHE, proving that the optics of the photocathode remains mainly unaffected by the platinum layer.

However, with respect to the ZnO/Ag back contact photocathode, the photocathode with ZnO/Ag/Pt back contact shows a significant shift in E_{onset} in positive bias direction (270 mV) and is measured to be 1765 mV versus RHE. Furthermore, an impressively high E_{MPP} of 1457 mV versus RHE is exhibited by the platinized photocathode, with a photocurrent density of 4.4 mA/cm^2, which accentuates both, the excellent catalytic activity of platinum as a catalyst for the hydrogen evolution reaction (HER) and its viable combination with the a-Si:H/a-Si:H/ZnO/Ag tandem device. In fact, the photocurrent density of 4.4 mA/cm^2 at 1457 mV versus RHE is the highest reported value at such positive potentials for a-Si:H single and tandem solar cell based photoelectrodes [13, 41–43]. Photocathodes, which can provide high photocurrents at more positive potentials, could effectively attenuate the catalytic activity requirement (i.e., reduction of overpotential losses) of the anode in a two-electrode PEC system. Taking additionally into account the nonideal illumination of the a-Si:H/a-Si:H photocathode by the halogen lamp, our result a fortiori demonstrates the capability for a direct application of the developed photocathodes in efficient and self-contained PEC devices. A prior study on amorphous tandem junction solar cell used as photocathode reported E_{onset} values of 1.35 V versus the saturated calomel electrode (SCE) along with a photocurrent

density of 2 mA/cm^2 at 0 V versus SCE [41]. A similar approach led to 1.43 V versus SCE and 3 mA/cm^2 at 0 V versus SCE [42]. Furthermore, this study reported on a tandem junction a-Si:H solar cell deposited on a crystalline silicon wafer. This triple cell concept promoted a high E_{onset} of 1.84 V versus RHE, but a rather low photocurrent density of 2.4 mA/cm^2. The most recent work focusing on the direct application of a-Si:H solar cells as photoelectrodes was done by Lin et al. [13]. Here, single junction a-Si:H solar cells were tested as photocathodes under the irradiation by a simulated sunlight (AM 1.5 light spectrum, 100 mW/cm^2) and exhibited an E_{onset} of 0.93 V versus RHE and photocurrent densities of 6.1 and 9.4 mA/cm^2 at 0.8 and 0.7 V versus RHE, respectively.

As integrated water splitting devices require chemical-resistant electrodes, stability issues of the silicon solar cells in contact with aqueous solutions need to be addressed and are currently under investigation. Furthermore, light induced degradation plays a major role for a-Si:H based devices and has been extensively investigated [18, 43]. In the present study this was not yet a focus of our work. It should however be noticed that the important parameter V_{OC} is typically the least affected parameter upon prolonged illumination and in some cases even increases [44].

4. Conclusion

We presented the development of a-Si:H/a-Si:H based photocathodes for efficient hydrogen production. By varying the substrate temperature and SiH_4 to total gas-flow concentration during the deposition of intrinsic a-Si:H absorber layers, we demonstrated that, in the case of a-Si:H/a-Si:H tandem cells, the optical and electrical properties of the a-Si:H subcells can be tuned and provide an extended V_{OC} range in tandem devices. It was found that the V_{OC} of tandem solar cells, with efficiencies around 10%, could systematically be adjusted between 1600 mV and 1870 mV.

Furthermore, the performance of the developed tandem junction solar cells as photocathodes was demonstrated in a PEC arrangement. In particular, a-Si:H/a-Si:H photocathodes with ZnO/Ag/Pt back contact exhibited excellent onset potentials over 1760 mV versus RHE with a photocurrent density of 5.3 mA/cm^2 at 0 V versus RHE and thus fulfill the main thermodynamic requirements to generate H_2. The presented approach exploits a strategy of an efficient and low-cost route to solar hydrogen production based on amorphous thin film silicon tandem junction solar cells at a level which is sufficient for technological use.

Conflict of Interests

The authors declare that there is no conflict of interests regarding the publication of this paper.

Acknowledgments

The authors thank J. Klomfaß, S. Tillmanns, L. Petter, W. Reetz, H. Siekmann, U. Gerhards, O. Thimm, and W. Beyer for their contributions to this work. The research is partly financially supported by the Deutsche Forschungsgemeinschaft (DFG) Prority Programme 1613: Regeneratively Produced Fuels by Light Driven Water Splitting: Investigation of Involved Elementary Processes and Perspectives of Technologic Implementation and by the Bundesministerium für Bildung und Forschung (BMBF) in the network project: Sustainable Hydrogen (FKZ 03X3581B). J. Ziegler, B. Kaiser, and W. Jaegermann acknowledge partial financial support by the DFG Excellency Graduate School of Energy Science and Engineering (GSC 1070).

References

[1] N. S. Lewis and D. G. Nocera, "Powering the planet: chemical challenges in solar energy utilization," *Proceedings of the National Academy of Sciences of the United States of America*, vol. 103, no. 43, pp. 15729–15735, 2006.

[2] J. P. Holdren, "Energy and sustainability," *Science*, vol. 315, no. 5813, p. 737, 2007.

[3] O. Khaselev and J. A. Turner, "A monolithic photovoltaic-photoelectrochemical device for hydrogen production via water splitting," *Science*, vol. 280, no. 5362, pp. 425–427, 1998.

[4] T. G. Deutsch, C. A. Koval, and J. A. Turner, "III-V nitride epilayers for photoelectrochemical water splitting: GaPN and GaAsPN," *The Journal of Physical Chemistry B*, vol. 110, no. 50, pp. 25297–25307, 2006.

[5] A. Heller and R. G. Vadimsky, "Efficient solar to chemical conversion: 12% efficient photoassisted electrolysis in the [p-type InP(Ru)]/HCl-KCl/Pt(Rh) cell," *Physical Review Letters*, vol. 46, no. 17, pp. 1153–1156, 1981.

[6] J. Ziegler, D. Fertig, B. Kaiser et al., "Preparation and characterization of GaP semiconductor electrodes for photoelectrochemical water splitting," *Energy Procedia*, vol. 22, pp. 108–113, 2012.

[7] A. Paracchino, V. Laporte, K. Sivula, M. Grätzel, and E. Thimsen, "Highly active oxide photocathode for photoelectrochemical water reduction," *Nature Materials*, vol. 10, no. 6, pp. 456–461, 2011.

[8] J. Y. Kim, G. Magesh, D. H. Youn et al., "Single-crystalline, wormlike hematite photoanodes for efficient solar water splitting," *Nature*, vol. 3, p. 2681, 2013.

[9] F. F. Abdi, L. Han, A. H. M. Smets, M. Zeman, B. Dam, and R. van de Krol, "Efficient solar water splitting by enhanced charge separation in a bismuth vanadate-silicon tandem photoelectrode," *Nature Communications*, vol. 4, article 3195, 2013.

[10] D. V. Esposito, I. Levin, T. P. Moffat, and A. A. Talin, "H_2 evolution at Si-based metal-insulator-semiconductor photoelectrodes enhanced by inversion channel charge collection and H spillover," *Nature Materials*, vol. 12, no. 6, pp. 562–568, 2013.

[11] J. R. McKone, E. L. Warren, M. J. Bierman et al., "Evaluation of Pt, Ni, and Ni-Mo electrocatalysts for hydrogen evolution on crystalline Si electrodes," *Energy and Environmental Science*, vol. 4, no. 9, pp. 3573–3583, 2011.

[12] U. Sim, T.-Y. Yang, J. Moon et al., "N-doped monolayer graphene catalyst on silicon photocathode for hydrogen production," *Energy & Environmental Science*, vol. 6, no. 12, pp. 3658–3664, 2013.

[13] Y. Lin, C. Battaglia, M. Boccard et al., "Amorphous Si thin film based photocathodes with high photovoltage for efficient hydrogen production," *Nano Letters*, vol. 13, no. 11, pp. 5615–5618, 2013.

[14] L. Han, F. F. Abdi, P. Perez Rodriguez et al., "Optimization of amorphous silicon double junction solar cells for an efficient photoelectrochemical water splitting device based on a bismuth vanadate photoanode," *Physical Chemistry Chemical Physics*, vol. 16, no. 9, pp. 4220–4229, 2014.

[15] S. Y. Reece, J. A. Hamel, K. Sung et al., "Wireless solar water splitting using silicon-based semiconductors and earth-abundant catalysts," *Science*, vol. 334, no. 6056, pp. 645–648, 2011.

[16] E. L. Miller, R. E. Rocheleau, and S. Khan, "A hybrid multijunction photoelectrode for hydrogen production fabricated with amorphous silicon/germanium and iron oxide thin films," *International Journal of Hydrogen Energy*, vol. 29, no. 9, pp. 907–914, 2004.

[17] A. Shah, *Thin-Film Silicon Solar Cells, Photovoltaics and Large-Area Electronics*, CRC Press, 2008.

[18] B. Rech and H. Wagner, "Potential of amorphous silicon for solar cells," *Applied Physics A*, vol. 69, no. 2, pp. 155–167, 1999.

[19] J. R. Bolton, S. J. Strickler, and J. S. Connolly, "Limiting and realizable efficiencies of solar photolysis of water," *Nature*, vol. 316, no. 6028, pp. 495–500, 1985.

[20] M. F. Weber and M. J. Dignam, "Splitting water with semiconducting photoelectrodes-efficiency considerations," *International Journal of Hydrogen Energy*, vol. 11, no. 4, pp. 225–232, 1986.

[21] A. J. Nozik, "Photoelectrochemistry: applications to solar energy conversion," *Annual Review of Physical Chemistry*, vol. 29, pp. 189–222, 1978.

[22] L. Ley, "Photoemission and optical properties," *Topics in Applied Physics*, vol. 56, pp. 61–168, 2005.

[23] W. Beyer and H. Wagner, "The role of hydrogen in a-Si:H—results of evolution and annealing studies," *Journal of Non-Crystalline Solids*, vol. 59-60, no. 1, pp. 161–168, 1983.

[24] M. G. Walter, E. L. Warren, J. R. McKone et al., "Solar water splitting cells," *Chemical Reviews*, vol. 110, no. 11, pp. 6446–6473, 2010.

[25] R. van de Krol and M. Grätzel, *Photoelectrochemical Hydrogen Production*, Springer, New York, NY, USA, 2012.

[26] D. E. Carlson and C. R. Wronski, "Amorphous silicon solar cell," *Applied Physics Letters*, vol. 28, no. 11, pp. 671–673, 1976.

[27] S. Guha, J. Yang, P. Nath, and M. Hack, "Enhancement of open circuit voltage in high efficiency amorphous silicon alloy solar cells," *Applied Physics Letters*, vol. 49, no. 4, pp. 218–219, 1986.

[28] W. Böttler, V. Smirnov, J. Hüpkes, and F. Finger, "Texture-etched ZnO as a versatile base for optical back reflectors with well-designed surface morphologies for application in thin film solar cells," *Physica Status Solidi (A)*, vol. 209, no. 6, pp. 1144–1149, 2012.

[29] N. Wyrsch, F. Finger, T. J. McMahon, and M. Vanecek, "How to reach more precise interpretation of subgap absorption spectra in terms of deep defect density in a-Si:H," *Journal of Non-Crystalline Solids*, vol. 137-138, part 1, pp. 347–350, 1991.

[30] G. Hodes, "Photoelectrochemical cell measurements: getting the basics right," *Journal of Physical Chemistry Letters*, vol. 3, no. 9, pp. 1208–1213, 2012.

[31] G. Ganguly and A. Matsuda, "Importance of surface processes in defect formation in a-Si:H," *Journal of Non-Crystalline Solids*, vol. 164–166, part 1, pp. 31–36, 1993.

[32] R. A. Street, *Hydrogenated Amorphous Silicon*, Cambridge Solid State Science Series, Cambridge University Press, Cambridge, UK, 1991.

[33] Y. Ashida, "Conference record of the 24th IEEE photovoltaic specialists conference," in *Proceedings of the IEEE 1st World Conference on Photovoltaic Energy Conversion*, vol. 1-2, 1994.

[34] A. Matsuda, *Tetrahedrally Bonded Amorphous Semiconductors*, pp. 192–196, American Institute of Physics, 1981.

[35] A. H. M. Smets, W. M. M. Kessels, and M. C. M. van de Sanden, "Vacancies and voids in hydrogenated amorphous silicon," *Applied Physics Letters*, vol. 82, no. 10, pp. 1547–1549, 2003.

[36] A. H. M. Smets and M. C. M. van de Sanden, "Relation of the Si-H stretching frequency to the nanostructural Si-H bulk environment," *Physical Review B*, vol. 76, no. 7, Article ID 073202, 2007.

[37] V. Smirnov, O. Astakhov, R. Carius, Y. Petrusenko, V. Borysenko, and F. Finger, "Variation in absorber layer defect density in amorphous and microcrystalline silicon thin film solar cells with 2MeV electron bombardment," *Japanese Journal of Applied Physics*, vol. 51, no. 2, Article ID 022301, 2012.

[38] V. Smirnov, O. Astakhov, R. Carius et al., "Performance of p- and n-side illuminated microcrystalline silicon solar cells following 2 MeV electron bombardment," *Applied Physics Letters*, vol. 101, Article ID 143903, 2012.

[39] S. Nakano, "High absorption-coefficient and stable a-Si for high-efficiency solar cells," in *Proceedings of the Conference Record of the 21st IEEE Photovoltaic Specialists Conference*, vol. 2, pp. 1656–1661, Kissimmee, Fla, USA, 1990.

[40] W. E. McMahon, K. E. Emery, D. J. Friedman et al., "Fill factor as a probe of current-matching for $GaInP_2$/GaAs tandem cells in a concentrator system during outdoor operation," *Progress in Photovoltaics: Research and Applications*, vol. 16, no. 3, pp. 213–224, 2008.

[41] M. Matsumura, Y. Sakai, S. Sugahara, Y. Nakato, and H. Tsubomura, "Photoelectrochemical hydrogen evolution using amorphous silicon electrodes having p-i-n or p-i-n-p-i-n junctions," *Solar Energy Materials*, vol. 13, no. 1, pp. 57–64, 1986.

[42] Y. Sakai, S. Sugahara, M. Matsumura, Y. Nakato, and H. Tsubomura, "Photoelectrochemical water splitting by tandem type and heterojunction amorphous silicon electrodes," *Canadian Journal of Chemistry*, vol. 66, no. 8, pp. 1853–1856, 1988.

[43] D. L. Staebler and C. R. Wronski, "Reversible conductivity changes in discharge-produced amorphous Si," *Applied Physics Letters*, vol. 31, no. 4, pp. 292–294, 1977.

[44] V. Smirnov, A. Lambertz, S. Tillmanns, and F. Finger, "p- and n-type microcrystalline silicon oxide (μc-SiO_x: H) for applications in thin film silicon tandem solar cells," *Canadian Journal of Physics*, vol. 92, pp. 932–935, 2014.